# Crystal structures of aldehyde deformylating oxygenase from *Limnothrix* sp. KNUA012 and *Oscillatoria* sp. KNUA011

Ae Kyung Park [a, 1], Il-Sup Kim [b, 1], Byung Wook Jeon [a], Soo Jung Roh [a], Min-Young Ryu [c], Hae-Ri Baek [c], Seoung-Woo Jo [d], Young-Saeng Kim [e], Hyun Park [a, f], Jun Hyuck Lee [a, f, **], Ho-Sung Yoon [b, c, ***], Han-Woo Kim [a, f, *]

[a] *Division of Polar Life Sciences, Korea Polar Research Institute, Incheon 21990, Republic of Korea*
[b] *School of Life Sciences, BK21 Plus KNU Creative BioResearch Group, Kyungpook National University, Daegu 41566, Republic of Korea*
[c] *Department of Biology, Kyungpook National University, Daegu 41566, Republic of Korea*
[d] *Department of Energy Science, Kyungpook National University, Daegu 41566, Republic of Korea*
[e] *Division of Biological Sciences, University of California San Diego, La Jolla, CA 92093-0116, USA*
[f] *Department of Polar Sciences, University of Science and Technology, Incheon 21990, Republic of Korea*

## ARTICLE INFO

## ABSTRACT

The cyanobacterial aldehyde deformylating oxygenase (cADO) is a key enzyme that catalyzes the unusual deformylation of aliphatic aldehydes for alkane biosynthesis and can be applied to the production of biofuel *in vitro* and *in vivo*. In this study, we determined crystal structures of two ADOs from *Limnothrix* sp. KNUA012 (LiADO) and *Oscillatoria* sp. KNUA011 (OsADO). The structures of LiADO and OsADO resembled those of typical cADOs, consisting of eight α-helices found in ferritin-like di-iron proteins. However, structural comparisons revealed that while the LiADO active site was vacant of iron and substrates, the OsADO active site was fully occupied, containing both a coordinated metal ion and substrate. Previous reports indicated that helix 5 is capable of adopting two distinct conformations depending upon the existence of bound iron. We observed that helix 5 of OsADO with an iron bound in the active site presented as a long helix, whereas helix 5 of LiADO, which lacked iron in the active site, presented two conformations (one long and two short helices), indicating that an equilibrium exists between the two states in solution. Furthermore, acquisition of a structure having a fully occupied active site is unique in the absence of higher iron concentrations as compared with other cADO structures, wherein low affinity for iron complicates the acquisition of crystal structures with bound iron. An in-depth analysis of the ADO apo-enzyme, the enzyme with substrate bound, and the enzyme with both iron and substrate bound provided novel insight into substrate-binding modes in the absence of a co-ordinated metal ion and suggested a separate two-step binding mechanism for substrate and iron co-factors. Moreover, our results provided a comprehensive structural basis for conformational changes induced by binding of the substrate and co-factor.

© 2016 Elsevier Inc. All rights reserved.

## 1. Introduction

Biofuels have drawn increasing attention as a renewable alternative-energy source to overcome climate change, the depletion of fossil fuels, and promote energy security. Specifically, fatty acid-derived alk(a/e)nes could be an ideal replacement for fossil-based fuel as a next-generation biofuel, because they are main constituents of traditional petro-based fuels (such as gasoline, diesel, and jet fuel), have high energy content, require minimal downstream processing, and have reduced $CO_2$ emissions [1].

Therefore, the study of alkane biosynthesis is of great interest, as it is an attractive target for large-scale biofuel production and open-pond systems. In nature, long-chain alkanes are commonly produced from fatty acid metabolites in microorganisms [2,3], insects, birds [4], plants [5], cyanobacteria, and green algae [6], where they function as waterproofing agents. Among these microorganisms, cyanobacteria- and algae-based biofuels are recognized as attractive options, because they can be grown under minimal nutrient requirements, used directly as biodiesel without undergoing transesterification [7], and are biodegradable and relatively environmentally friendly [8,9].

Specifically, cyanobacteria are appealing due to their well-established genetic engineering platform for lipid-based production of biofuel products and their ability to effectively convert solar energy and carbon dioxide into biofuels [10–12]. Recently, two genes involved in the alkane-biosynthesis pathway from cyanobacteria were identified [3], wherein acyl-acyl-carrier protein reductase (AAR) converts free fatty acids to fatty aldehydes, and then aldehyde-deformylating oxygenase (ADO) catalyzes conversion of $C_n$ fatty aldehydes to the corresponding $C_{n-1}$ alkanes/alkenes and formate by cleavage of the bond between the aldehyde carbon and the $\alpha$-carbon [13]. Although alkanes are very simple molecules, the reaction associated with their conversion from aldehyde is a difficult and unusual transformation [14]. Therefore, ADO has attracted a great deal of attention for potential biotechnological applications based on its ability to catalyze this complicated reaction. ADOs were originally identified as metal-dependent integral membrane proteins with a molecular weight of ~70 kDa that converted the aldehyde carbon to carbon monoxide in higher plants and green algae and to carbon dioxide in insects [16]. Recently, cyanobacterial ADO (cADO) was identified as a soluble protein with an approximate molecular weight of 30 kDa that is also relatively easy to purify and express in recombinant form [3].

Because of the amenability of the enzyme, cADO crystal structures were determined, revealing their membership in the non-heme di-nuclear iron-oxygenase family of enzymes that includes methane monooxygenase, type I ribonucleotide reductase, and ferritin [15–21]. All of the structures contain a di-iron center at the core of the protein, with the iron atoms coordinated by two histidine and four carboxylate residues, which is similar to structural features observed in other di-iron oxygenases [15,17]. Additionally, all cADO structures were determined with bound aliphatic acid, which mimics the binding of the aldehyde substrate. This substrate analogue could possibly be bound or trapped by hydrophobic channels in *Escherichia coli* cells [19–21].

Another interesting feature of cADO is its poor *in vitro* activity, which yields only three to five catalytic turnovers per active site [18,22–25]. Oxygen- and auxiliary reducing systems (protein-based or chemical) are required for ADO activity, and given that the native redox partners of ADOs are unknown, determination of an efficient electron-transfer system is important for ADO activity [26]. In an effort to overcome the low activity of cADO, Wang et al. [27] constructed self-sufficient ADO systems, wherein ADO was fused with cognate ferredoxin-NADP$^+$ reductase and ferredoxin, resulting in cADO variants exhibiting a 3-fold increase in activity as compared with native cADO [26]. Additionally, previous reports involving ADO iron content in *Prochlorococcus marinus* (PmADO) and inductively coupled plasma optical-emission spectrometry analysis on *Synechococcus elongates* strain PCC7942 (SeADO) indicated that ADO bound iron atoms with low affinity, which might constitute an explanation for the low enzymatic activity observed in cADOs [19]. The requirement of a redox partner(s) and low iron content could significantly limit cADO applications in biofuel biotechnology; therefore, insight into cADO structure and mechanisms might facilitate their deployment in bioprocesses capable of generating renewable biofuels, including alk(a/e)ne and hydrocarbon fuels, in cyanobacteria or other heterologous bacterial hosts [27].

To elucidate more detailed information regarding ADO mechanisms, we solved crystal structures of two cADOs from *Limnothrix* sp. KNUA012 (LiADO) and *Oscillatoria* sp. KNUA011 (OsADO). Our results enhance the understanding of the ADO-mediated reaction mechanism, including the identification of bound substrate, the modes of action involving the substrate, and accessory factors that could potentially aid ADO engineering and production.

## 2. Materials and methods

### 2.1. Identification and cloning of cADO genes

*Oscillatoria* sp. KNUA011 and *Limnothrix* sp. KNUA012 isolated from fresh water in South Korea were cultured for 7 days at 25 °C in BG-11 medium (Sigma-Aldrich, St. Louis, MO, USA) adjusted to pH 7.0 in a controlled growth chamber (16-h light/8-h dark cycle, 70 $\mu$mol m$^{-2}$ s$^{-1}$). Cell pellets were harvested by centrifugation and prepared for genomic DNA isolation using a DNA/RNA Isolation Kit (Qiagen, Hilden, Germany) combined with glass beads. Genes encoding LiADO and OsADO were identified by GenomeWalker Universal Kit (Clontech, Mountain View, CA, USA) and PCR amplified using adaptor and gene-specific primers according to manufacturer instructions. The primers used were as follows: LiADO-F (5′-GAATTCACCTATGCGCAACTCGAG-3′), LiADO-R (5′-GTCGACTGGTGGTTAAGCGGCAGCG-3′), OsADO-F (5′-GAATTCATCTATGCCCCAGCTTGAG-3′), and OsADO-R (5′-GTCGACTTCGGAAATAAGGAATGGGA-3′). PCR conditions were as follows: initial denaturation at 94 °C for 3 min; 30 cycles at 94 °C for 30 s, 54 °C for 30 s, and 72 °C for 1.5 min; and final extension at 72 °C for 7 min. PCR products were purified using a Gel-Extraction Kit (Nucleogen, Danwon-Gu, South Korea) and then inserted into the TOPO-TA cloning vector (Invitrogen, Carlsbad, CA, USA). The cloned plasmid was sequenced using the M13 primer set to confirm that no PCR-induced mutations had been introduced, after which it was digested with *Eco*RI and *Sal*I restriction enzymes. The digested fragment was ligated into the *E. coli* expression vector pET28a(+) (Novagen, Madison, WI, USA), and the resulting plasmids were named pET28a(+):LiADO and pET28a(+):OsADO, respectively. *E. coli* NiCo21(DE3) cells were transformed with either pET28a(+):LiADO or pET28a(+):OsADO, and positive transformants were grown on Luria-Bertani agar plates supplemented with 50 $\mu$g/mL kanamycin for 24 h at 37 °C. The strains containing the transformed plasmid (pET28a(+):LiADO or pET28a(+):OsADO) were used for subsequent protein expression.

### 2.2. Protein expression and purification

The transformed *E. coli* cells were grown to an optical density at 600 nm of ~0.4, followed by induction of protein expression by the addition of 0.2 mM isopropyl $\beta$-D-1-thiogalactopyranoside. The cells were cultured for 20 h at 20 °C with shaking at 200 rpm. The cell pellet was harvested by centrifugation at 4000×$g$ for 20 min at 4 °C and resuspended in cold lysis buffer [20 mM Tris-HCl (pH 7.2), 300 mM NaCl, and 10 mM imidazole] containing 0.2 mg/mL lysozyme, 0.5 mM phenylmethylsulfonyl fluoride, and EDTA-free protease inhibitor cocktail (PIC; Sigma-Aldrich). After incubation for 30 min on ice, the cells were disrupted by ultrasonication with short pulses (10 s) and pauses (10 s) for 1 h using a Sonic Disembrator 550 (Thermo Fisher Scientific, Waltham, MA, USA) on ice, and the cell debris was removed by centrifugation at 12,000×$g$ for 30 min at 4 °C. The cleared supernatant was poured into a gravity-flow column containing Ni-NTA resin (Qiagen) pre-equilibrated

with lysis buffer. The histidine-tag-fused proteins (LiADO and OsADO) in the supernatant were bound to the Ni-NTA resin, and the unbound proteins were eluted with 10 column volumes of wash buffer containing 20 mM Tris-HCl (pH 7.2), 300 mM NaCl, and 20 mM imidazole. LiADO and OsADO proteins were eluted with elution buffer containing 20 mM Tris-HCl (pH 7.2), 300 mM NaCl, and 250 mM imidazole. Desalting and concentration determination of the LiADO and OsADO proteins was performed using cold 20 mM Tris-HCl (pH 7.2) with PIC in Amicon Ultra Centrifugal Filters (Ultracel-10K; Millipore, Billerica, MA, USA) according to manufacturer instructions. The resulting proteins were concentrated to ~40 mg/mL for crystallization trials. Protein concentrations were spectrophotometrically determined using protein dye reagent (Bio-Rad, Hercules, CA, USA).

### 2.3. Enzyme-activity assays

To measure ADO activity, enzyme mixtures consisted of 50 mM Tris-HCl (pH 7.4), 1 mM hexadecanal or octadecanal dissolved in dimethyl sulfoxide, 30 μM of purified LiADO or OsADO, 50 μg/mL ferredoxin (Sigma-Aldrich), 0.1 U/mL ferredoxin reductase (Sigma-Aldrich), 1 mM NADPH, and 10 μM ferrous ammonium sulfate (Sigma-Aldrich). Each reaction mixture was adjusted to 200 μL and reacted for 2 h at 37 °C with shaking at 200 rpm before being stopped by addition of an equal volume of ethyl acetate. Gas chromatography-mass spectrometry (GC-MS) analysis was performed as reported previously [21]. Concentrations of the catalytic products pentadecane and heptadecane (Sigma-Aldrich) were determined by GC-MS analysis by quantifying a standard curve of known concentrations of heptadecane and pentadecane. Residual amount of hexadecanal or octadecanal as substrates were also determined by GC-MS by quantifying an internal standard of known concentrations of hexadecanal or octadecanal (Tokyo Chemical Industry Co., Ltd, Tokyo, Japan).

### 2.4. PDB accession number

The coordinates of the structures together with the structure factors were deposited in the PDB (http://www.rcsb.org/pdb) with accession codes 5K52 and 5K53.

## 3. Results and discussion

### 3.1. LiADO and OsADO structures

LiADO and OsADO crystal structures were determined at resolutions of 2.4 Å and 1.8 Å, respectively, and were similar to previously reported ADO structures (Fig. 1A) [19–21]. These structures exhibited typical ADO-like structural characteristics, including eight α-helices. There were four and two molecules in the LiADO and OsADO asymmetric units, respectively. The LiADO and OsADO amino acid sequences are shown in Fig. 2, along with the sequence-specific locations of the α-helices; alignment of the LiADO and OsADO sequences indicated a shared identity of 69.5%. Interestingly, orthologues of the *ado* gene have only been found in cyanobacteria [28], and multiple-sequence alignment indicated that the ADO amino acid sequence is well conserved throughout cyanobacteria. The residues comprising the substrate channel and iron-binding site are also well conserved in both LiADO and OsADO, with Tyr21, Ile27, Val28, Phe67, Phe86, Phe87, Phe117, Ala118, Ala121, Tyr122, Try125, and Tyr184 contributing to substrate binding, and Glu32, Glu60, His63, Glu115, Glu144, and His147 participating in iron coordination.
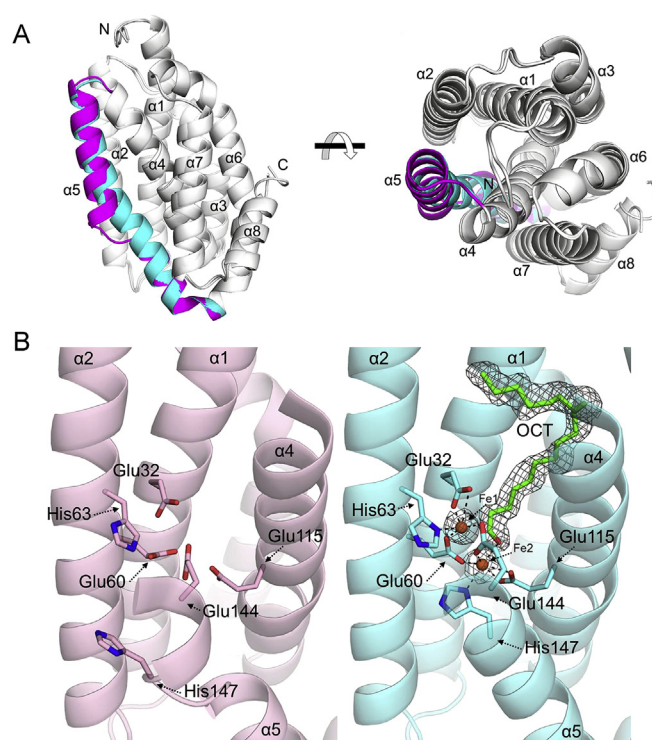


**Fig. 1.** (a) Two orthogonal views of the superposition of LiADO with OsADO_OCT. For clarity, only helix 5 is colored as magenta (LiADO) and cyan (OsADO_OCT). (b) Close-up view of the iron and substrate binding site of LiADO (pink) and OsADO_OCT (cyan). In OsADO_OCT, the bound iron ions and octadecanal are shown as spheres and stick model, respectively and electron density map are presented. The map as calculated with $(2|F_o|-|F_c|)$ and contoured at 1.5 σ. (For interpretation of the references to colour in this figure legend, the reader is referred to the web version of this article.)

In a previous report concerning SeADO, Jia et al. [20] solved structures representing five stages of the reaction process associated with ADOs by introducing point mutations, soaking the crystals in $H_2O_2$, or adding additional iron ions to the screens [19]. They distinguished structural differences based on the character of the bound ligand and the coordination mode of the iron atoms and observed conformational changes in Glu144, which is located in helix 5, induced by substrate binding. Helix 5 presented both as a long helix or as an extended stretch of residues unwound in the middle, resulting in two short helices connected by a loop in the SeADO structures, suggesting that conformational changes in helix 5 might correlate with loss of the di-iron cluster. This was supported by the PmADO crystal structure, which displayed a disordered helix 5 in the absence of bound iron ions [21].

Although LiADO and OsADO shared similar sequence homology and overall architecture with previously reported ADOs [19,21], they displayed difference active site conformations. Comparison of the LiADO and OsADO structures with that of SeADO suggested that LiADO and OsADO exhibit two different states of reaction processing, respectively. In contrast to currently available ADO structures displaying either or both iron ions and a long-chain substrate, two of the four LiADO molecules contained neither metal ions nor substrate (Fig. 1B). Therefore, we postulated that the LiADO structure represented an early stage of activity characterized by a vacant binding pocket. However, the OsADO active site displayed two bound iron ions and a fatty alcohol substrate, despite the absence of additional ion or introduction of point mutations that would
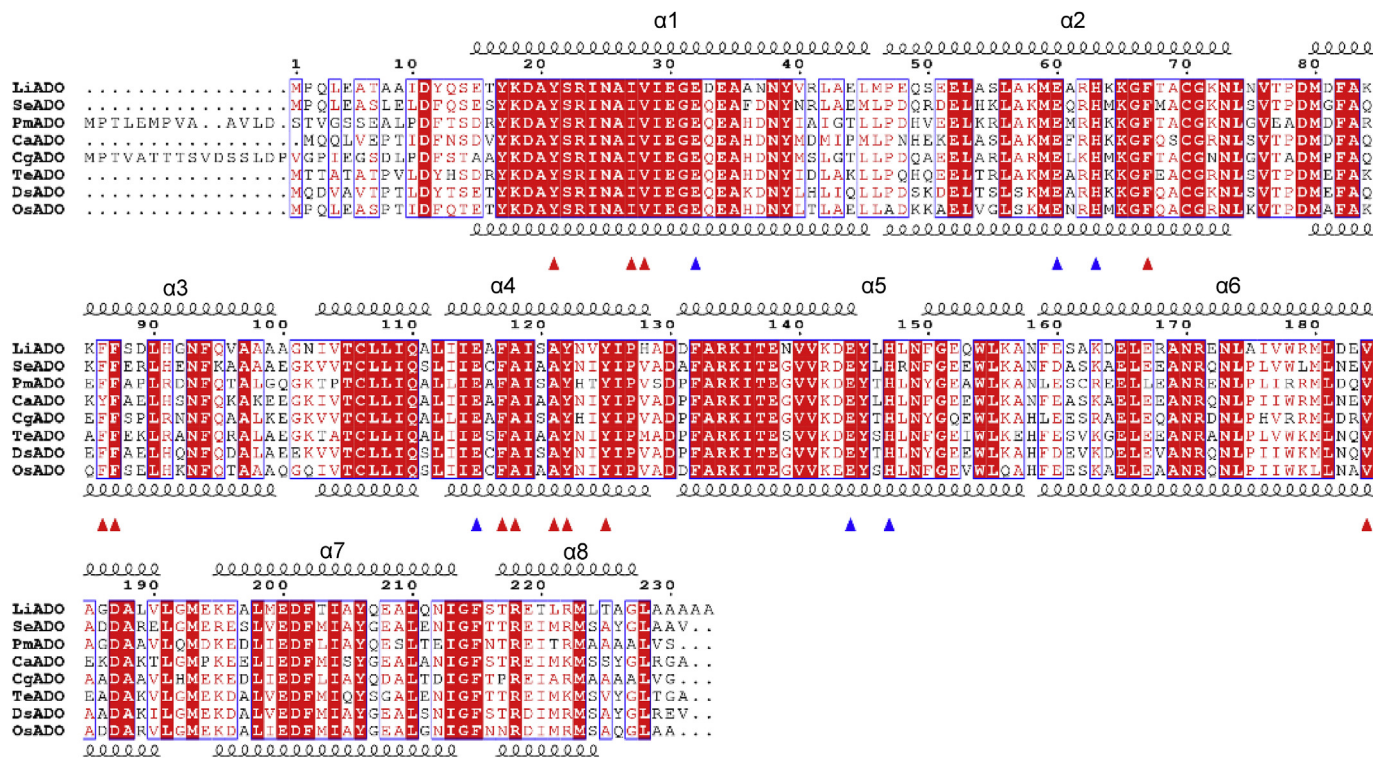
**Fig. 2.** The multiple amino acid sequence alignment of the ADOs. Secondary structure elements of LiADO and OsADO are labeled above and bottom of the sequences, respectively. The residues participating the substrate binding channel are highlighted by blue triangles and residues contributing the iron binding are highlighted by red triangles. The information of amino acid sequences are as follows: LiADO from *Limnothrix* sp. KNUA012 (GenBank code KX302881; SeADO from *Synechococcus elongatus* (UniProtKB code Q54764); PmADO from *Prochlorococcus marinus* (UniProtKB code Q7V6D4); CaADO from *Cyanobacterium aponinum* (UniProtKB code K9Z5G1); CqADO from *Cyanobium gracile* (UniProtKB code K9P3X5); TeADO from *Thermosynechococcus elongates* (UniProtKB code Q8DJB4); DsADO from *Dactylococcopsis salina* (UniProtKB code K9YV86); OsADO from *Oscillatoria* sp. KNUA011 (GenBank code KX302880). (For interpretation of the references to colour in this figure legend, the reader is referred to the web version of this article.)

promote substrate binding.

### 3.2. The LiADO structure resembles ADO structures with an empty active site

Of the four molecules in the LiADO asymmetric unit, none contained iron ions. Among the four molecules, electron density maps showed octadecanal bound in molecules A and C (Fig. 3A). The lack of electron density for coordinated iron in these molecules might be explained by previous metal analysis of cADOs, indicating their low affinity for iron ions [18], and SeADO structures that did not reflect fully occupied di-iron sites, despite incubation with additional iron [19]. As previously mentioned, bound iron correlates with a specific helix-5 conformation in ADO structures, implying that the helix-5 conformation in the LiADO structure should be distorted. However, our analysis indicated that LiADO helix 5 adopted both of two conformations by virtue of His147 orientation in helix 5 in all four molecules (Fig. 3A). We could fit the entire unwound version of helix 5 to the electron density map, while the long, continuous version of helix 5 only allowed proper positioning of residues Leu146 and His147 in the electron density map. This suggested equilibrium in the helix-5 conformation between the two different states observed among the four molecules in solution. However, the strong electron density associated with the area surrounding the distorted helix 5 suggested that the absence of the di-iron cluster altered helix-5 conformation, thereby eliminating the ability of the enzyme to coordinate the metal ion [19].

LiADO molecules B and D exhibited no electron density

indicating presence of the substrate, which was in contrast to other reported cADO structures, all of which contained a synthetic variation of the aliphatic fatty acid, except for the Y122F-mutant structure of SeADO [19–21]. Therefore, our observation of a vacant substrate-binding pocket in a cADO structure is unusual. However, in the A and C molecules, we observed electron density indicating presence of the bound substrate. Superimposition of substrate-bound apo-variants of LiADO over these molecules B and D revealed no significant structural differences (Fig. 4). In the SeADO structure, Glu144 underwent conformation changes upon substrate binding [19], while in the LiADO structure, Glu144 maintained the same orientation in both substrate configurations and interacted with the bound substrate along with Glu60 and Glu115.

### 3.3. OsADO structure resembles ADO structures with active sites containing both metal co-factor and substrate

While the active site in each LiADO molecule was vacant, those of each OsADO molecule were fully occupied. There were two molecules in the OsADO asymmetric unit, with the active site of each containing both an iron ion and the substrate. This structure was referred to as OsADO_OCT, given that structural and biochemical analysis indicated that the bound ligand was octadecanal. Interestingly, despite not increasing the iron concentration of the solution during crystal preparation, OsADO exhibited strong electron density associated with the iron ions (Fig. 1B), suggesting that OsADO might exhibit a greater affinity for iron relative to that observed in other cADOs. To determine whether this increased
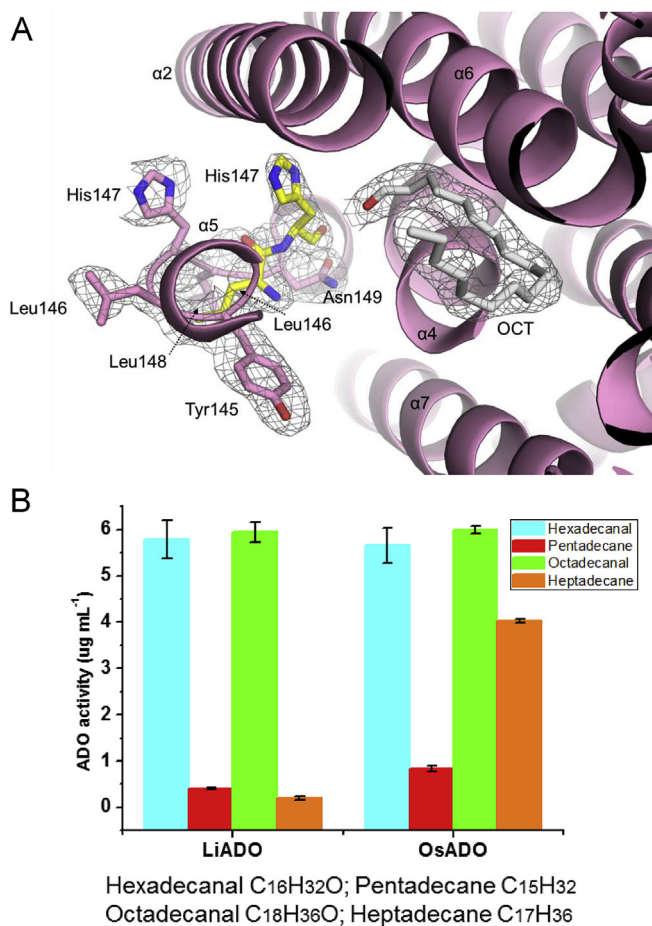
Fig. 3. (a) Close-up view of the helix 5 of LiADO (pink). Note that ordered helix 5 of LiADO is colored as yellow. The bound substrate and residues 145–149 are shown as stick model and presented as electron density map. The map as calculated with $(2|F_o|-|F_c|)$ and contoured at 1.5 σ. (b) Enzymatic activity of LiADO and OsADO through comparison of the effects of both substrates. Enzymatic activity was measured by GC/MS analysis as described in *Materials and Methods*. (For interpretation of the references to colour in this figure legend, the reader is referred to the web version of this article.)

affinity correlated with higher enzymatic activity, we measured the catalytic activities of LiADO and OsADO using hexadecanal ($C_{16}$ aldehyde) and octadecanal ($C_{18}$ aldehyde) as substrates (Fig. 3B). Our results indicated that both enzymes displayed similar activity in the presence of hexadecanal, but OsADO exhibited 8-fold higher activity in the presence of octadecanal as compared with that observed for LiADO. Furthermore, OsADO exhibited a 5-fold greater efficiency at processing the octadecanal substrate than that observed for processing the hexadecanal substrate. Previous studies reported broad substrate specificity demonstrated by PmADO, ranging from $C_4$ to $C_{18}$ aldehydes and exhibiting maximal activity in the presence of octadecanal. However, PmADO activity in the presence of octadecanal was only 2-fold higher than that observed in the presence of hexadecanal [20]. These results suggested that ADOs exhibit different catalytic activities despite high degrees of shared sequence identity, and that this might be explained by differing affinities for metal co-factors.

Comparison of the OsADO_OCT structure with that of SeADO_WT1 (SeADO_OCT) [19] revealed a difference in Glu144 conformation (Fig. 4). In the SeADO structure, it adopts a position oriented outward and away from the active site, precluding its ability to coordinate metal ions. However, in the OsADO_OCT structure, the Glu144 side chain is oriented into the active site and is involved in the coordination of two iron ions. This observation indicated that in the OsADO_OCT structure, Glu144 conformation promoted metal coordination and might represent the state prior to Glu44 conformational alteration following catalysis. In the OsADO_OCT structure, the Fe1 ion is penta-coordinated by conserved Glu32, Glu60, His63, and Glu144 residues, while the Fe2 ion is penta-coordinated by conserved Glu60, Glu115, Glu144, and His147 residues and interactions with the bound substrate. This structural conformation was different from that observed in the SeADO_OCT structure, wherein each iron ion exhibited a distorted tetrahedral coordination.

In conclusion, our structural and functional analysis of LiADO and OsADO suggested that improved metal (iron)-binding affinity can enhance ADO catalytic activity and potentially augment lipid-based biofuel production to attain high levels of efficiency in industrial and scientific fields.
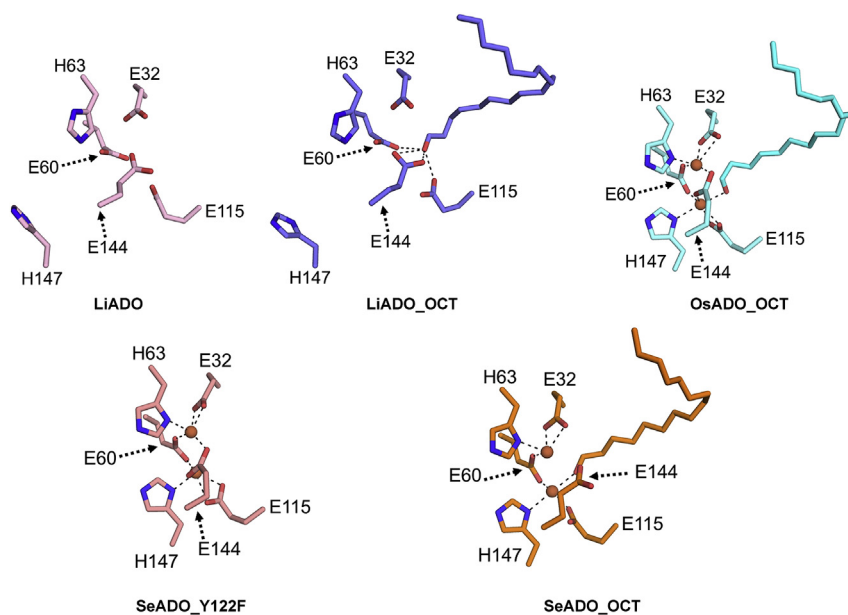


Fig. 4. Substrate binding site comparison of LiADO and OsADO with SeADO. For clarity, only conserved 6 residues (E32, E60, H63, E115, E144 and H147), bound iron ions and substrate are presented. The structures of LiADO, LiADO_OCT, OsADO_OCT, SeADO_Y122F and SeADO_OCT are shown in pink, blue, cyan, salmon, and orange, respectively. (For interpretation of the references to colour in this figure legend, the reader is referred to the web version of this article.)

## Acknowledgement

## Transparency document

Transparency document related to this article can be found online at http://dx.doi.org/10.1016/j.bbrc.2016.06.090.

## Appendix A. Supplementary data

Supplementary data related to this article can be found at http://dx.doi.org/10.1016/j.bbrc.2016.06.090.

## References

[1] Y.J. Choi, S.Y. Lee, Microbial production of short-chain alkanes, Nature 502 (2013) 571—574.

[2] V.M. Dembitsky, M. Srebnik, Variability of hydrocarbon and fatty acid components in cultures of the filamentous cyanobacterium Scytonema sp isolated from microbial community "black cover" of limestone walls in Jerusalem, Biochemistry (Mosc.) 67 (2002) 1276—1282.

[3] A. Schirmer, M.A. Rude, X.Z. Li, E. Popova, S.B. del Cardayre, Microbial biosynthesis of alkanes, Science 329 (2010) 559—562.

[4] J.A. Tillman, S.J. Seybold, R.A. Jurenka, G.J. Blomquist, Insect pheromones - an overview of biosynthesis and endocrine regulation, Insect Biochem. Mol. Biol. 29 (1999) 481—514.

[5] L. Samuels, L. Kunst, R. Jetter, Sealing plant surfaces: cuticular wax formation by epidermal cells, Annu. Rev. Plant Biol. 59 (2008) 683—707.

[6] J. Chang, J.W. Hong, H. Chae, H.S. Kim, K.M. Park, K.I. Lee, H.S. Yoon, Natural production of alkane by an easily harvested freshwater cyanobacterium, Phormidium autumnale KNUA026, Algae 28 (2013) 93—99.

[7] J. Yang, X. Ming, Z. Xuezhi, H. Qiang, S. Milton, C. Yongsheng, Life-cycle analysis on biodiesel production from microalgae: water footprint and nutrients balance, Bioresour. Technol. 102 (2011) 159—165.

[8] A. Demirbas, Biodiesel from oilgae, biofixation of carbon dioxide by microalgae: a solution to pollution problems, Appl. Energy 88 (2011) 3541—3547.

[9] A.H. Demirbas, Inexpensive oil and fats feedstocks for production of biodiesel, Energy Educ. Sci. Technol. Part A-Energy Sci. Res. 23 (2009) 1—13.

[10] I.M.P. Machado, S. Atsumi, Cyanobacterial biofuel production, J. Biotechnol. 162 (2012) 50—56.

[11] X.F. Lu, A perspective: photosynthetic production of fatty acid-based biofuels in genetically engineered cyanobacteria, Biotechnol. Adv. 28 (2010) 742—746.

[12] J.J. Zhang, X.F. Lu, J.J. Li, Conversion of fatty aldehydes into alk (a/e)nes by in vitro reconstituted cyanobacterial aldehyde-deformylating oxygenase with

[13] the cognate electron transfer system, Biotechnol. Biofuels 6 (2013), 86.

[13] L.J. Rajakovich, H. Norgaard, D.M. Warui, W.C. Chang, N. Li, S.J. Booker, C. Krebs, J.M. Bollinger, M.E. Pandelia, Rapid reduction of the diferric-peroxyhemiacetal intermediate in aldehyde-deformylating oxygenase by a cyanobacterial ferredoxin: evidence for a free-radical mechanism, J. Am. Chem. Soc. 137 (2015) 11695—11709.

[14] P.H. Buist, Exotic biomodification of fatty acids, Nat. Prod. Rep. 24 (2007) 1110—1127.

[15] M.H. Baik, M. Newcomb, R.A. Friesner, S.J. Lippard, Mechanistic studies on the hydroxylation of methane by methane monooxygenase, Chem. Rev. 103 (2003) 2385—2419.

[16] J. Stubbe, D.G. Nocera, C.S. Yee, M.C.Y. Chang, Radical initiation in the class I ribonucleotide reductase: long-range proton-coupled electron transfer? Chem. Rev. 103 (2003) 2167—2201.

[17] E.C. Theil, D.J. Goss, Living, With iron (and oxygen): questions and answers about iron homeostasis, Chem. Rev. 109 (2009) 4568—4579.

[18] D. Das, B.E. Eser, J. Han, A. Sciore, E.N.G. Marsh, Oxygen-independent decarbonylation of aldehydes by cyanobacterial aldehyde decarbonylase: a new reaction of diiron enzymes, Angew. Chem. Int. Ed. Engl. 50 (2011) 7148—7152.

[19] C.J. Jia, M. Li, J.J. Li, J.J. Zhang, H.M. Zhang, P. Cao, X.W. Pan, X.F. Lu, W.R. Chang, Structural insights into the catalytic mechanism of aldehyde-deformylating oxygenases, Protein Cell 6 (2015) 55—67.

[20] B. Khara, N. Menon, C. Levy, D. Mansell, D. Das, E.N.G. Marsh, D. Leys, N.S. Scrutton, Production of propane and other short-chain alkanes by structure-based engineering of ligand specificity in aldehyde-deformylating oxygenase, Chembiochem 14 (2013) 1204—1208.

[21] B.C. Buer, B. Paul, D. Das, J.A. Stuckey, E.N.G. Marsh, Insights into substrate and metal binding from the crystal structure of cyanobacterial aldehyde deformylating oxygenase with substrate bound, ACS Chem. Biol. 9 (2014) 2584—2593.

[22] B.E. Eser, D. Das, J. Han, P.R. Jones, E.N.G. Marsh, Oxygen-independent alkane formation by non-heme iron-dependent cyanobacterial aldehyde decarbonylase: investigation of kinetics and requirement for an external electron donor, Biochemistry 50 (2011) 10743—10750.

[23] N. Li, W.C. Chang, D.M. Warui, S.J. Booker, C. Krebs, J.M. Bollinger, Evidence for only oxygenative cleavage of aldehydes to alk(a/e)nes and formate by cyanobacterial aldehyde decarbonylases, Biochemistry 51 (2012) 7908—7916.

[24] C. Andre, S.W. Kim, X.H. Yu, J. Shanklin, Fusing catalase to an alkane-producing enzyme maintains enzymatic activity by converting the inhibitory byproduct H2O2 to the cosubstrate O2, Proc. Natl. Acad. Sci. U. S. A. 110 (2013) 3191—3196.

[25] D.M. Warui, N. Li, H. Norgaard, C. Krebs, J.M. Bollinger, S.J. Booker, Detection of formate, rather than carbon monoxide, as the stoichiometric coproduct in conversion of fatty aldehydes to alkanes by a cyanobacterial aldehyde decarbonylase, J. Am. Chem. Soc. 133 (2011) 3316—3319.

[26] Q. Wang, X.N. Huang, J.J. Zhang, X.F. Lu, S.Y. Li, J.J. Li, Engineering self-sufficient aldehyde deformylating oxygenases fused to alternative electron transfer systems for efficient conversion of aldehydes into alkanes, Chem. Commun. 50 (2014) 4299—4301.

[27] M.E. Pandelia, N. Li, H. Norgaard, D.M. Warui, L.J. Rajakovich, W.C. Chang, S.J. Booker, C. Krebs, J.M. Bollinger Jr., Substrate-triggered addition of dioxygen to the diferrous cofactor of aldehyde-deformylating oxygenase to form a diferric-peroxide intermediate, J. Am. Chem. Soc. 135 (2013) 15801—15812.

[28] S. Klahn, D. Baumgartner, U. Pfreundt, K. Voigt, V. Schon, C. Steglich, W.R. Hess, Alkane biosynthesis genes in cyanobacteria and their transcriptional organization, Front. Bioeng. Biotechnol. 2 (2014) 24.